Strain Fields

25

CHAPTER PREVIEW

As we discussed in Chapter 23, bending of the lattice planes causes a change in the diffraction conditions and therefore a change in the contrast of the image. The presence of a lattice defect in the specimen causes the planes to bend close to the defect. The special feature here is that the bending varies not just laterally, but also through the specimen. Since the details of the bending generally depend on the characteristics of the defect, we can learn about the defect by studying the contrast in the TEM image. This simple principle has led to one of the main applications of TEM, namely, the study of defects in crystalline materials. We can claim that our understanding of the whole field of dislocations and interfaces, for example, has advanced because of TEM. We have even discovered new defects using TEM.

Usually we want to learn two things about these defects: we want to know where they are and then understand what they are. So the idea underlying this chapter is the same as for bend contours: we use different reflections corresponding to different sets of lattice planes. We see how the defects affect the image contrast from those different lattice planes and thus characterize the defects. In case you are worried, we would like to emphasize that this is *not* a chapter about defects, it is concerned with understanding contrast in the TEM. We will introduce the necessary terminology and notation concerning defects, but we won't try to give you a com-

D. B. Williams et al., *Transmission Electron Microscopy*

prehensive discussion of them. You should consult the standard references on dislocations at the end of the chapter if you need more details. However, we will show lots of pictures because now we are concerned with the appearance of images.

Strain Fields

25

25.1. WHY IMAGE STRAIN FIELDS?

First, we should review our terminology. When we displace the atom at position **r** a distance **R**(**r**) from its site in the perfect crystal, we say the crystal is under a strain (ε). If the crystal is strained then it must be subject to a stress, which we'll call σ. (Metallurgists traditionally use these symbols and although σ means "cross section" to a microscopist, we'll stick with it.) Since **R**(**r**) varies with position in the crystal, ε and σ will in general also vary with **r**. We will assume that ε and σ can each be defined at a point. Then we will refer to these quantities as the displacement field, **R**(**r**), the strain field, ε(**r**), and the stress field, σ(**r**). You will notice that these terms are used interchangeably in the literature. What we image is the effect of the **R**(**r**).

To have an intuitive feel for why we see contrast from dislocations, consider the geometry shown in Figure 25.1. The diffraction geometry has been set up so that the specimen is slightly tilted away from the Bragg condition. The distortion due to the dislocation will then bend the near-diffracting planes back into the Bragg-diffracting condition. We have relrods so there will still be some intensity in the electron beam even when we are not at the exact Bragg condition. The figure shows planes bending at a dislocation; compare this to Figure 23.7 showing bend contours. Regions far from the dislocation are tilted well away from the Bragg condition, while the regions either side of the dislocation core are at the Bragg condition for $\pm\,\mathbf{g}_{hk\ell}$. It is more difficult to "see" the diffracting planes for a screw dislocation (Figure 25.2A) but the effect is the same.

When studying a particular dislocation (edge or screw), we want to determine the following parameters:

- The direction and magnitude of the Burgers vector, **b**, which is normal to the $hk\ell$ diffracting planes (Figures 25.1 and 25.2B).
- The line direction (a vector) and therefore the character of the dislocations (edge, screw, or mixed).
- The glide plane.

There are other questions we want to answer:

- Is the dislocation interacting with other dislocations, or with other lattice defects?
- Is the dislocation jogged, kinked, or straight?
- What is the density of dislocations in that region of the specimen (and what was it before we prepared the specimen)?
- Has the dislocation adopted some special configuration, such as a helix?

In many of these questions, you may find that stereomicroscopy (Section 31.1) can be very helpful, although we will not emphasize that technique. The basic requirement if you do use stereomicroscopy is that you must form all of your images using the same **g**-vector.

25.2. HOWIE–WHELAN EQUATIONS

Let's start with the two-beam phenomenological approach because it worked so well in Chapter 24. An important assumption is that we have linear elasticity. What this means is that if we have $\mathbf{R}_1$ due to one defect and $\mathbf{R}_2$ due to a second defect, then at any point in the specimen we can just add these two values to determine the total displacement field, **R**. We will not consider anisotropic elasticity, although this can readily be included in calculations.

In Chapter 24, we showed that we could modify the Howie–Whelan equations to include a lattice distortion **R**. So for the imperfect crystal

$$\frac{d\phi_{\mathbf{g}}}{dz} = \frac{\pi i}{\xi_{\mathbf{0}}}\phi_{\mathbf{g}} + \frac{\pi i}{\xi_{\mathbf{g}}}\phi_{\mathbf{0}} \exp\left[-2\pi i\left(sz + \mathbf{g}\cdot\mathbf{R}\right)\right] \qquad [25.1]$$

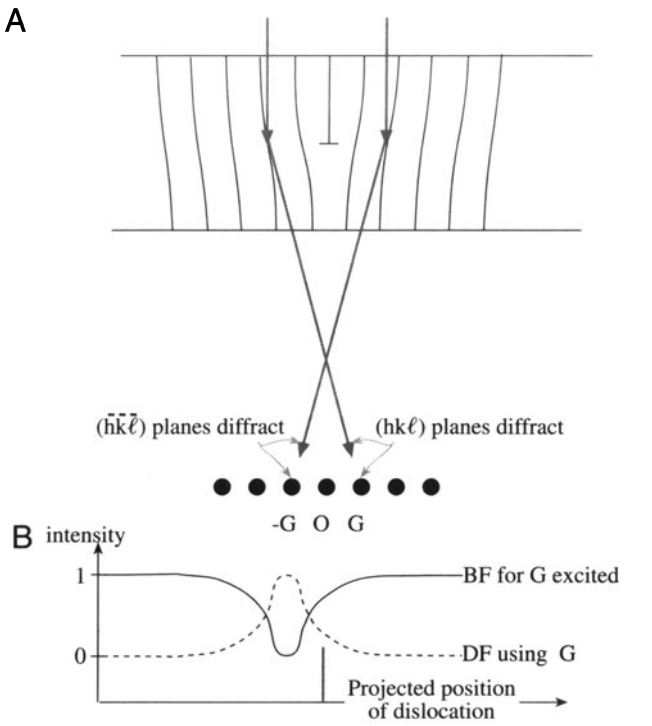

Figure 25.1. (A) The specimen is tilted slightly away from the Bragg condition ($\mathbf{s} \neq 0$). The distorted planes close to the edge dislocation are bent back into the Bragg-diffracting condition ($\mathbf{s} = 0$), diffracting into G and –G as shown. (B) Schematic profiles across the dislocation image showing that the defect contrast is displaced from the projected position of the defect.

Now we make a different substitution of variables (compare with equations 24.5 and 24.6). Set

$$\phi_0(z)_{(\text{sub})} = \phi_0(z) \exp\left(\frac{-\pi i z}{\xi_0}\right) \qquad [25.2]$$

and

$$\phi_{\mathbf{g}}(z)_{(\text{sub})} = \phi_{\mathbf{g}} \exp\left(2\pi i s z - \frac{\pi i z}{\xi_0} + 2\pi i\, \mathbf{g}\cdot\mathbf{R}\right) \qquad [25.3]$$

The justification for this substitution is the same as always. You'll notice that $\phi_0(z)_{(\text{sub})}$ is the same as before, but $\phi_{\mathbf{g}(\text{sub})}$ now includes a $\mathbf{g}\cdot\mathbf{R}$ term. The reason for this substitution is that it will give us a simple expression for $d\phi_{\mathbf{g}}/dz$.

The equations become

$$\frac{d\phi_0(z)_{(\text{sub})}}{dz} = \frac{\pi i}{\xi_{\mathbf{g}}}\phi_{\mathbf{g}}(z)_{(\text{sub})} \qquad [25.4]$$

and

$$\frac{d\phi_{\mathbf{g}(\text{sub})}}{dz} = \frac{\pi i}{\xi_{\mathbf{g}}}\phi_0(z)_{(\text{sub})} + \left[2\pi i\left(s + \mathbf{g}\cdot\frac{d\mathbf{R}}{dz}\right)\right]\phi_{\mathbf{g}}(z)_{(\text{sub})} \qquad [25.5]$$

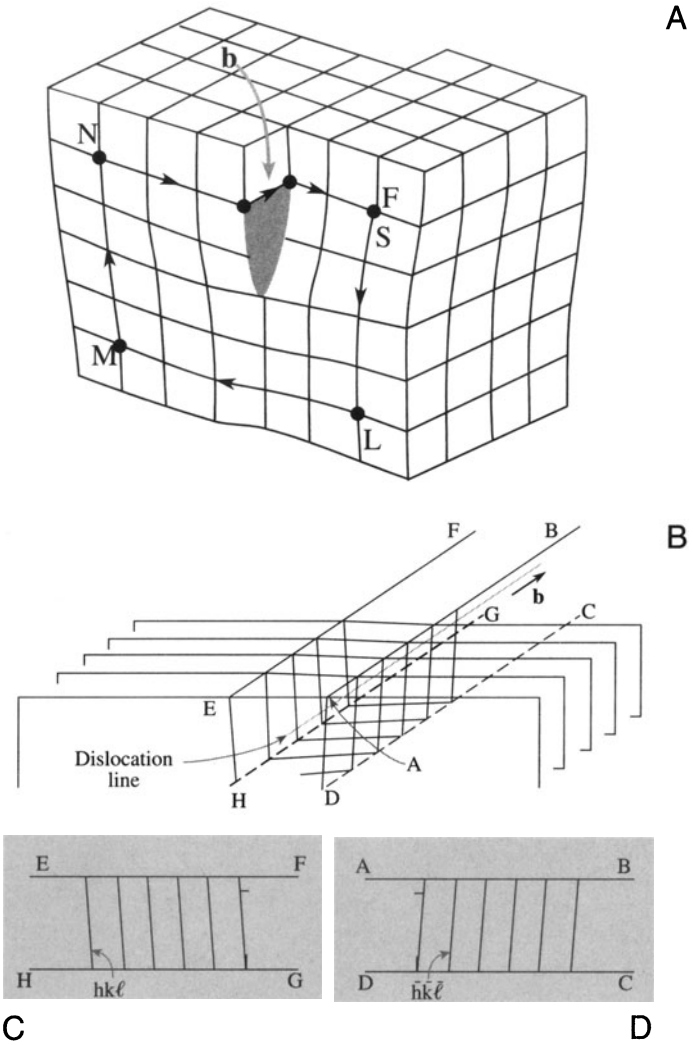

Figure 25.2. (A) Distortion of planes around a screw dislocation. The circuit SLMNF is used to define the Burgers vector, **b** (see Figure 25.5). (B) Schematic showing the rotation of the diffracting planes by a screw dislocation. The planes are rotated in opposite directions on either side (C, D) of the dislocation.

which can be rewritten, while dropping the subscript

$$\frac{d\phi_{\mathbf{g}}}{dz} = \frac{\pi i}{\xi_{\mathbf{g}}}\phi_0 + 2\pi i s_{\mathbf{R}}\phi_{\mathbf{g}} \qquad [25.6]$$

This equation looks just like equation 13.14 but with $s_{\mathbf{R}}$ instead of s, where

$$s_{\mathbf{R}} = s + \mathbf{g}\cdot\frac{d\mathbf{R}}{dz} \qquad [25.7]$$

The concept of $s_{\mathbf{R}}$ is new.

The importance of this result is that although we have a new "s," we have the same equation so we can use the rest of the analysis of Chapter 13 and obtain the same results with a modified value of s, i.e., $s_{\mathbf{R}}$. Therefore, we'll

have the same thickness dependence so that the contrast of the defects will depend on both s and ξ_g. The big change is that we can now treat the case where **R** is a continuous function of z.

We will examine how the $\mathbf{g}\cdot d\mathbf{R}/dz$ and $\mathbf{g}\cdot\mathbf{R}$ terms are used to understand dislocations. Since the equations we have just derived have the same form as those we discussed in Chapters 11 and 24, we can expect many of the same properties in the images. In particular, the images of defects will show the same sort of thickness dependence. We can also use the equations we derived in Chapter 24, so we have two ways of looking at the defects:

- $\mathbf{g}\cdot\mathbf{R}$ contrast is used when **R** has a single value,
- $s_{\mathbf{R}}$ contrast is used when **R** is a continuously varying function of z,

which in turn is associated with $\mathbf{g}\cdot d\mathbf{R}/dz$.

Now let's consider the principles of this analysis. Remember, we are not trying to be quantitative or totally rigorous. We will generalize the two-beam treatment for the imperfect crystal. Note that we still have beams, it's a dynamical situation, and we assume that the column approximation is valid (Hirsch *et al.* 1960). So how does the column approximation relate to the theory? The model relates **R** to the column, as shown in Figure 25.3, and the calculation is for a continuum even though we have atoms. The important point is that for a displacement field, **R** varies with position, **r**; we can define the origin as the core of the defect. We'll go through the calculation for a dislocation parallel to the foil surface.

As we saw in Section 13.11, the column approximation is equivalent to assuming that the crystal can be divided into narrow columns. We then calculate the amplitudes of the beams in any such column as if the whole crystal consisted of an infinite number of identical columns. The approximation is valid when we don't need to see image detail below ~2–3 nm. The actual diameter of the column depends on the diffracting conditions (Howie and Basinski 1968; Howie and Sworn 1970). We can include the effect of distortions due to strains from lattice defects by imagining that the column consists of slabs of perfect crystal each displaced by an amount **R**(z) (see Section 24.13). Remember that z is actually measured along the column.

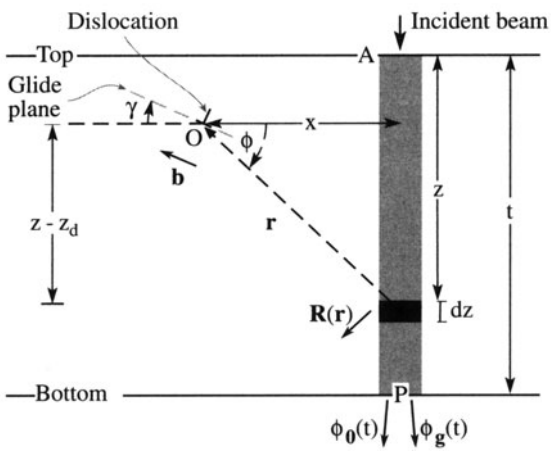

Figure 25.3. The effect of a dislocation with Burgers vector, **b,** at O on a column, distance x away. The effect of the strain field on the electron waves in the column is integrated in increments dz over its total length t, giving amplitudes $\phi_0(t)$ and $\phi_g(t)$ at P.

25.3. CONTRAST FROM A SINGLE DISLOCATION

When we study dislocations, we usually want to know how many there are (the density) and whether they are edge, screw, or mixed in character. The displacement field in an isotropic solid for the general, or mixed, case (Hirth and Lothe 1982) can be written as

$$\mathbf{R} = \frac{1}{2\pi}\left(\mathbf{b}\phi + \frac{1}{4(1-\nu)}\{\mathbf{b}_e + \mathbf{b}\times\mathbf{u}(2(1-2\nu)\ln r + \cos 2\phi)\}\right) \quad [25.8]$$

For convenience, **R** is given here in polar coordinates (r and ϕ) shown in Figure 25.3; **b** is the Burgers vector, $\mathbf{b}_e$ is the edge component of the Burgers vector, **u** is a unit vector along the dislocation line (the line direction), and ν is Poisson's ratio.

It was particularly important to be able to write down this expression when we did the calculations by hand. However, when we have a computer available, it's quite straightforward to use anisotropic elasticity (Steeds 1973) or just feed in displacements calculated from a computer model of the atom structure.

The amplitude of the diffracted beam, ϕ_g, is directly influenced by the value of **R**. We can consider two particular cases, namely, the screw and edge dislocations. For the screw dislocation, $\mathbf{b}_e = 0$ and **b** is parallel to **u** so that $\mathbf{b}\times\mathbf{u} = 0$. Then the expression for **R** in equation 25.8 simplifies to

$$\mathbf{R} = \mathbf{b}\frac{\phi}{2\pi} = \frac{\mathbf{b}}{2\pi}\tan^{-1}\left(\frac{z-z_d}{x}\right) \quad [25.9]$$

Here, z is the distance traveled down the column and z_d is the distance of the dislocation core below the top surface (again, refer to Figure 25.3). The dependence on $(z - z_d)$ emphasizes that the displacement field is present above

Table 25.1. Different Burgers Vectors and Different Reflections Give Different g·b = *n* Values[a]

g \ b	$\frac{1}{6}[11\bar{2}]$	$\frac{1}{6}[1\bar{2}1]$	$\frac{1}{6}[\bar{2}11]$	$\frac{1}{3}[111]$
$\pm(1\bar{1}1)$	± 1/3	± 2/3	± 1/3	± 1/3
$\pm(\bar{1}\bar{1}1)$	± 2/3	± 1/3	± 1/3	± 1/3
$\pm(0\bar{2}2)$	± 1	± 1	0	0
±(200)	± 1/3	± 1/3	± 2/3	± 2/3
$\pm(3\bar{1}1)$	0	± 1	± 1	± 1
$\pm(\bar{3}\bar{1}1)$	± 1	0	± 1	± 1

[a]The dislocations all lie on a (111) plane in an fcc material; the beam direction is [011].

and below the dislocation; it affects the whole column. From these two equations we see that **g·R** is proportional to **g·b**. For this reason, we often discuss images of dislocations in terms of **g·b** (g-dot-b) contrast. Examples of **g·b** values for some dislocations lying on a (111) plane in an fcc material with a [011] beam direction are given in Table 25.1.

The second special case arises when the dislocation is pure edge in character. Then $\mathbf{b} = \mathbf{b}_e$ and **g·R** involves two terms, **g·b** and **g·b×u**. (The latter term is read as "g-dot-b-cross-u.") The displacement field causes the Bragg-diffracting planes associated with **g** to bend. Incidentally, the origin of **g·b×u** is interesting; it arises because the glide plane is buckled by the presence of an edge dislocation (Hirth and Lothe 1982) as illustrated in Figure 25.4. This buckling can be important because it complicates the analysis of **b** for some dislocations with an edge component, as we'll see below.

- Always remember: **g·R** causes the contrast and for a dislocation, **R** changes with *z*.
- We say that **g·b** = *n*. If we know **g** and we determine *n*, then we know **b**.

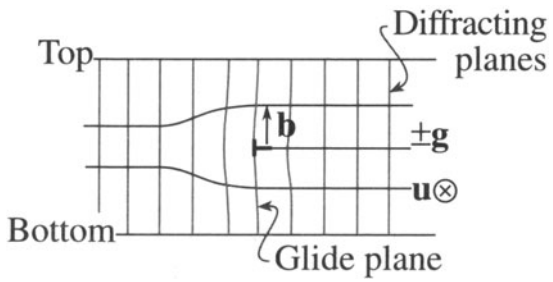

Figure 25.4. Buckling of the glide planes arises because of the term **g·b×u** and is important because it complicates the analysis of **b**.

An experimental point: you usually set *s* to be greater than 0 when imaging a dislocation. Then the dislocation can appear dark against a bright background in a BF image. Of course, you still need to think about $s_{\mathbf{R}}$ and $d\mathbf{R}/dz$ since these will vary with *z*, as we saw in Figure 25.1.

The + and – signs in Table 25.1 are very important. If the sign of **R**, and hence **g·R** or **g·b**, reverses, then the image of the dislocation will move to the other side of the projected position of the dislocation core. If you look carefully at Figure 25.1, you can appreciate that reversing the sign of *s* produces the same effect as reversing the sign of **g**. We can summarize these two ideas in terms of the quantity (**g·b**)*s* ("g-dot-b-times-s"), as shown in Figure 25.5.

If **g·b** = 0 , then you won't see any contrast because the diffracting planes are then parallel to **R**. This is termed the *invisibility criterion.*

If we identify two reflections, $\mathbf{g}_1$ and $\mathbf{g}_2$, for which **g·b** = 0, then $\mathbf{g}_1 \times \mathbf{g}_2$ is parallel to **b**. This identification of **b** is actually a little more complicated because dislocations appear out of contrast when **g·b** < 1/3; similarly, dislocations need not be invisible even if **g·b** = 0 when **g·b×u** ≠ 0. Further exceptions to the rule are given in Edington (1976).

If we compare the contrast from a dislocation with that from a SF, the difference is that now α is a continuously varying function of *z*. The image of the dislocation itself shows thickness fringes, but it may be "out of contrast" at some depths or thicknesses, as you can see in the experimental image shown in Figure 25.6A.

Some points to remember from this discussion are:

- The sign of *s* affects the image.
- The sign of *x* affects the image; the image is asymmetric.
- The magnitude of **s** affects the image.
- The depth of the dislocation and the thickness of the specimen affect the image.
- The appearance of the image depends on **g·b** or, more completely, on (**g·b**)*s* and **g·b×u**.
- If we repeat this analysis for other values of **g·b** (= *n*) and plot intensities, we would find that the image width becomes broader as *n* increases.
- Note where the dislocation image "comes from": the position of the line in the image only rarely corresponds to the projected position of the dislocation; it is usually displaced to one side of the core.
- As a complication, remember that the dislocations will probably be found in wedge specimens, not ideal parallel-sided ones.

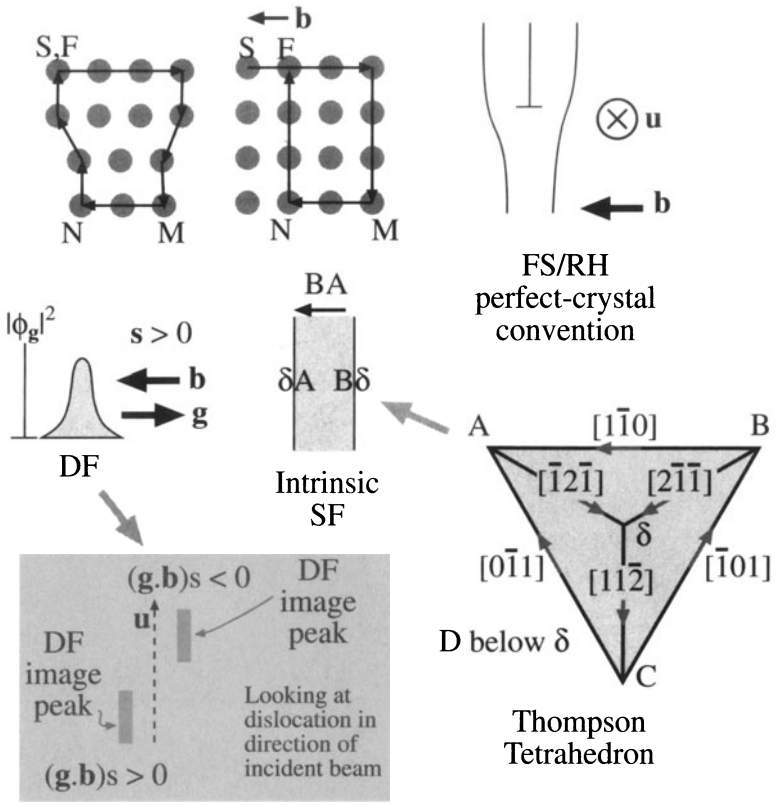

Figure 25.5. A brief summary of dislocations in an fcc crystal: **b** is defined by the finish- (F) to-start (S) vector in a right-hand (RH) circuit that comes to closure around the dislocation but fails to close in the perfect crystal. The location of the diffracted intensity $|\phi_g|^2$ relative to the core depends on the sign of **b**, **g**, and *s* for the FSRH convention. If any sign is reversed, the contrast shifts across the core. When a perfect dislocation splits into Shockley partial dislocations, the order of the partial dislocations is given by the Thompson tetrahedron.

A final "rule of thumb" which you may find useful (from computer modeling and early analytical calculations) is

> If **g**·**b** = 0, you can still "see" dislocations when **g**·**b**×**u** ≥ 0.64. For fcc materials, this rule can be useful when the foil is not parallel to a {111} plane.

Other examples of dislocation images are illustrated in Figure 25.6. Remember that partial dislocations are not only present in fcc metals; they also occur in many fcc semiconductors and many layer materials. Such materials may have a very low stacking-fault energy allowing the partial dislocations to separate, forming wide ribbon-like defects, as shown in Figures 25.6A–C. The single line below the arrow in (C) is a dislocation having its Burgers vector parallel to **g** here (so **g**·**b** = 2); you can see two "peaks" in the image, one darker and broader than the other. Notice that one peak has nearly disappeared in (B) and the broad peak is on the other side of the dislocation. A group of three parallel lines is present in (C) but is out of contrast in (B). These are three Shockley partial dislocations all having the same **b** and thus all giving **g**·**b** = 0 in (B) (the three lines actually form by the dissociation of a perfect dislocation with Burgers vector $\frac{1}{2}$<112>). The 11$\bar{1}$ image (A) is formed by tilting the specimen to a 112 pole (~20° from the 111 pole) and shows contrast from the stacking faults themselves; these faults will never give contrast at the 111 pole since **g**·**R** is then always 0 (or an integer). The intermetallics tend to have large unit cells so that the superlattice dislocations dissociate into partial dislocations, which would have been perfect dislocations in the disordered crystal (Figures 25.6D and E). These super-partial dislocations can dissociate further as they might have in the disordered lattice, or they can separate differently in different ordered domains (Figure 25.6F). Dislocations in interphase boundaries can be revealed by imaging with different reflections (Figures 25.6G and H). Since the dislocations are present to accommodate the mismatch, they must lie at, or close to, the (001) phase boundary. It can be difficult to analyze their Burgers vectors unambiguously, because the adjoining materials have different extinction distances, etc. One of the extra challenges is determining the plane on which this dissociation occurs. We'll illustrate how we can see **g**·**b**×**u** contrast when we examine dislocation loops in Zn in Section 25.6.

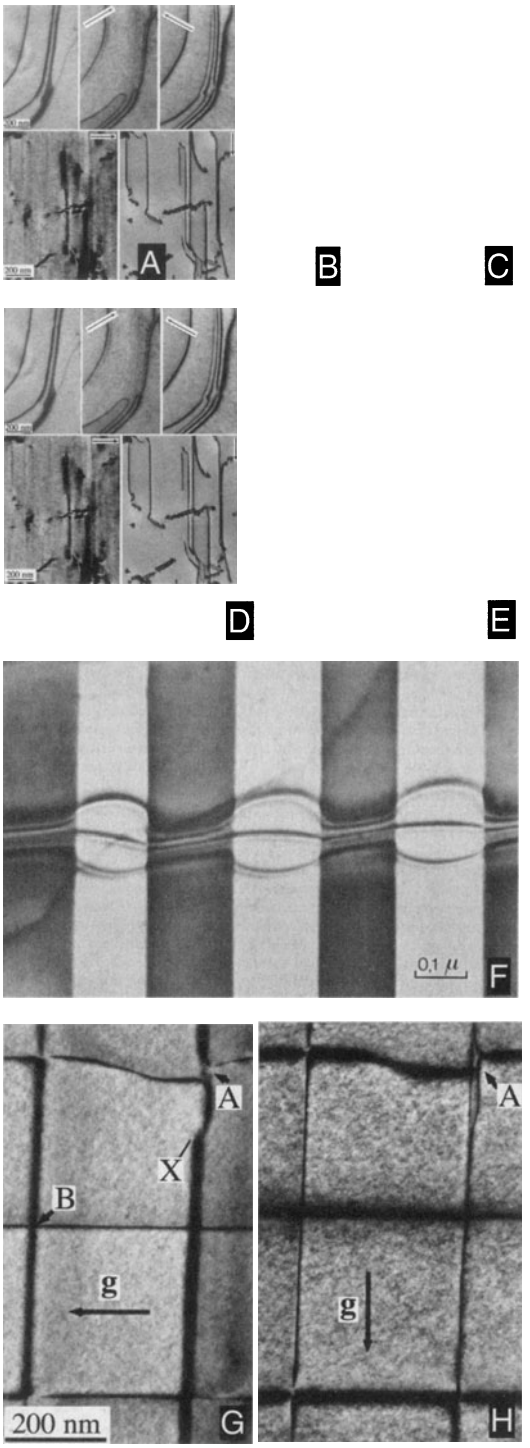

Figure 25.6. (A–C) Three strong-beam BF images from the same area using (A) {11$\bar{1}$} and (B,C) {220} reflections to image dislocations which lie nearly parallel to the (111) foil surface in a Cu alloy which has a low stacking-fault energy. (D,E) Dislocations in Ni_3Al in a (001) foil imaged in two orthogonal {220} reflections. Most of the dislocations are out of contrast in (D). (F) A complex dislocation crossing a (rotational) domain boundary; the character of the dislocation changes and thus its dissociation width changes. (G,H) Dislocations in a (001) interface between two slightly lattice-mismatched III-V compounds.

25.4. DISPLACEMENT FIELDS AND EWALD'S SPHERE

In Section 25.3, we showed that when a displacement $\mathbf{R}(\mathbf{r})$ is present, we can think of s as being replaced by $s_{\mathbf{R}}$ (equation 25.7). Hirsch *et al.* (1977) (see also Goringe 1975) showed that this new s should be written more completely as

$$s_{\mathbf{R}} = s + \mathbf{g} \cdot \frac{\partial \mathbf{R}}{\partial z} + \theta_B \mathbf{g} \cdot \frac{\partial \mathbf{R}}{\partial x} \qquad [25.10]$$

The point is that, as you can see in Figure 25.7, $\mathbf{R}$ causes the lattice planes to bend through an angle $\delta\phi$. So two other parameters, namely, $\mathbf{g}$ and s, also change. The diffraction vector is actually lengthened by $\Delta\mathbf{g}$ but, more importantly, $\mathbf{g}$ is rotated. The result is that s increases by the two com-

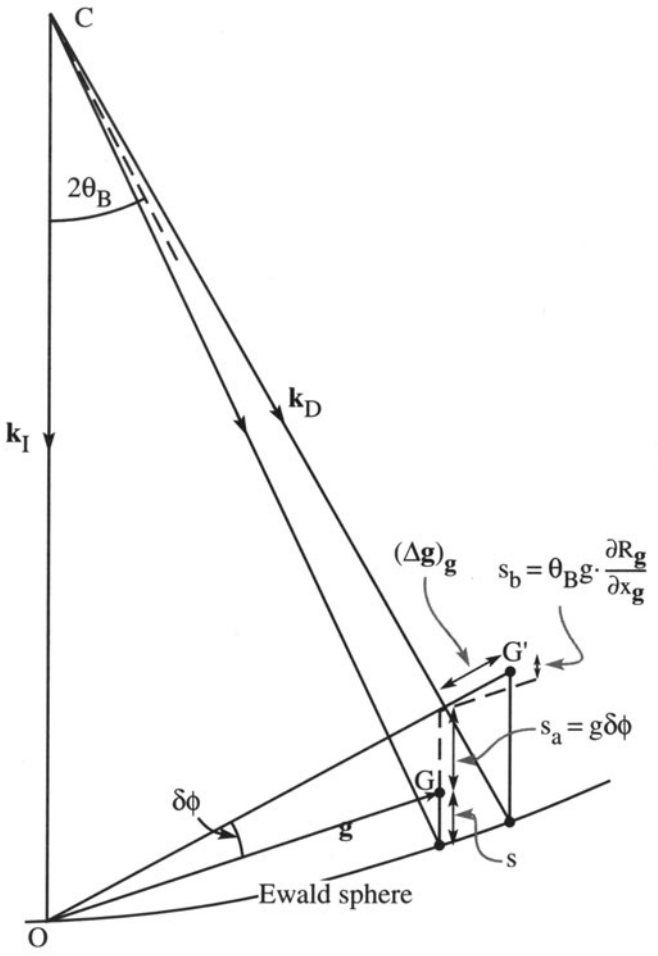

Figure 25.7. The strain field of the dislocation causes the lattice planes to bend through an angle $\delta\phi$. So $\mathbf{g}$ and s also change. The diffraction vector is lengthened by $\Delta\mathbf{g}$ and $\mathbf{g}$ is rotated. So s increases by the two components of $s_{\mathbf{R}}$, i.e., s_a and s_b.

ponents, s_a and s_b, shown in the figure, to give s_R. If you manipulate this equation for small angles you produce equation 25.8. We usually neglect the third term because θ_B is small, but it can become important when screw dislocations intersect the surface (Tunstall *et al.* 1964).

An alternative way of looking at this deformation is to think of **g** as changing by $\Delta\mathbf{g}$. We can define this change by the equation

$$\mathbf{g} \cdot \left(\mathbf{r} - \mathbf{R}(\mathbf{r})\right) = \left(\mathbf{g} + \Delta\mathbf{g}\right) \cdot \mathbf{r} \qquad [25.11]$$

so that

$$-\mathbf{g} \cdot \mathbf{R}(\mathbf{r}) = \Delta\mathbf{g} \cdot \mathbf{r} \qquad [25.12]$$

The implication is that the information about the displacement field, $\mathbf{R}(\mathbf{r})$, is present in the region around **g** but not actually at **g**. Remember that the reflection **g** is present because we have a perfect crystal. It is difficult to image this type of scattering. If you displace the objective aperture, you will still see the dislocation, but other inelastic scattering will complicate image interpretation. We saw that scattering does indeed occur between Bragg reflections in Section 17.6. An analogy for scattering from dislocations is the scattering of light from a single slit which we discussed in Chapter 2.

In the deformable-ion approximation (Section 24.13), we make the assumption that the atom doesn't know it has moved. If $\mathbf{R}(\mathbf{r})$ varies rapidly, as it does near the core of a dislocation, the approximation must fail. You can draw the same conclusion whenever the density of the material changes rapidly. So what we should do is use a better model for the atomic potential, one that also takes account of what happens to the valence electrons at such a defect. Of course, linear elasticity theory also fails when the strains, and hence $\mathbf{R}(\mathbf{r})$, are large, as at dislocation cores.

25.5. DISLOCATION NODES AND NETWORKS

You can analyze the Burgers vectors of dislocations which form networks directly and easily, if all the dislocations lie in a plane parallel to the surface of the specimen, as illustrated in Figure 25.8 for the case of graphite. The idea is simple: you form a series of images using different **g**-vectors. Don't forget that you can tilt to other poles; in fact, you'll often need to tilt the specimen just to image SFs which lie parallel to the foil surface, as in Figure 25.8A. Such tilting experiments are essential if you're examining networks of misfit dislocations, since the dislocations will then often have a component of their Burgers vector out of the plane of the network.

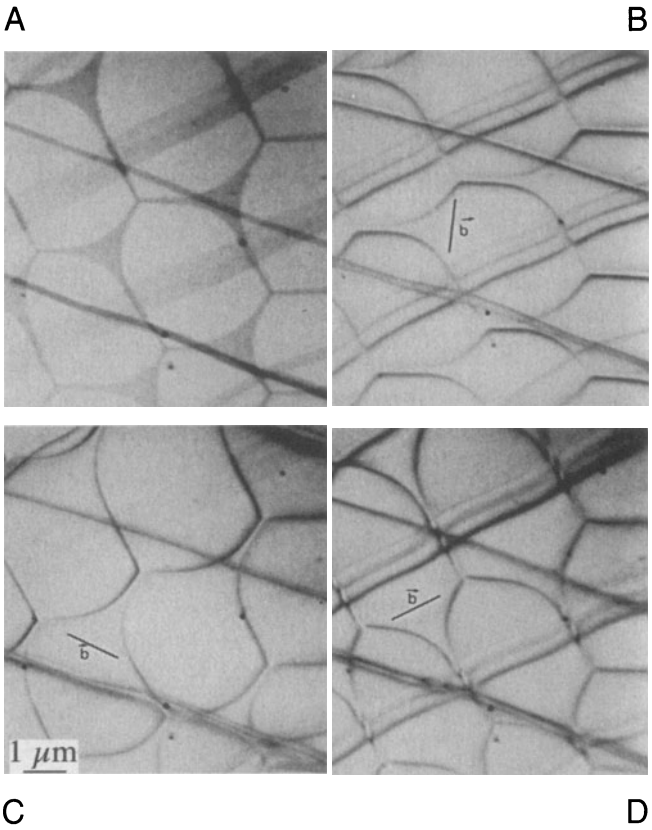

Figure 25.8. Dislocation networks in graphite. In (A) the stacking faults parallel to the foil surface are imaged, in (B), (C), and (D) two of the three dislocations at each node are in contrast but the third is invisible. Knowing **g** for each image, the Burgers vector of the dislocations can be determined as shown.

25.6. DISLOCATION LOOPS AND DIPOLES

Loops have been studied extensively because they can form when point defects coalesce. There are probably thousands of papers describing TEM studies of radiation damage and the formation of dislocation loops. In fact, many HVEMs were built in the 1960s just to study this problem. Questions which were answered led to a greatly improved understanding of irradiation processes (but failed to justify the construction of more nuclear power stations). We found that:

- The loops can form by coalescence of interstitials or vacancies.
- The rate of growth, critical size, and nucleation time for different loops can be measured.

- Some of the loops are faulted (containing a SF) while others are not faulted. The faulting should be related to the size of the loop and the stacking-fault energy of the material.

These studies were particularly instructive illustrations of the value of diffraction contrast.

- Dislocation loops can have either positive or negative **b**, as shown in Figure 25.9.
- Loops can be present which show no **g**·**b** contrast.
- Loops can enclose single or multiple stacking faults, and so exhibit SF contrast as shown in Figure 25.10.
- The dislocation dipole is a special case and gives an important example of interacting dislocations. TEM is the best way to image dipoles because they have no long-range strain fields; the Burgers vector of the complete dipole is zero!

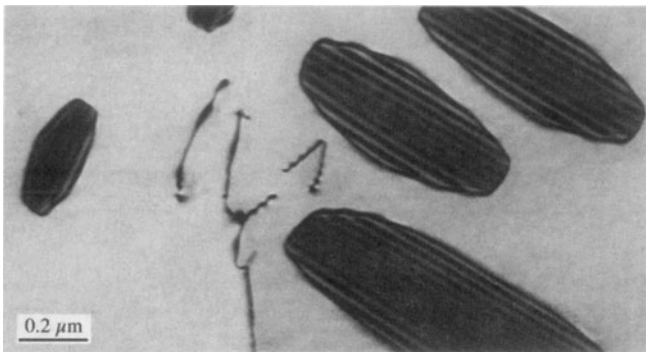

Figure 25.10. Dislocation loops in irradiated Ni showing SF contrast.

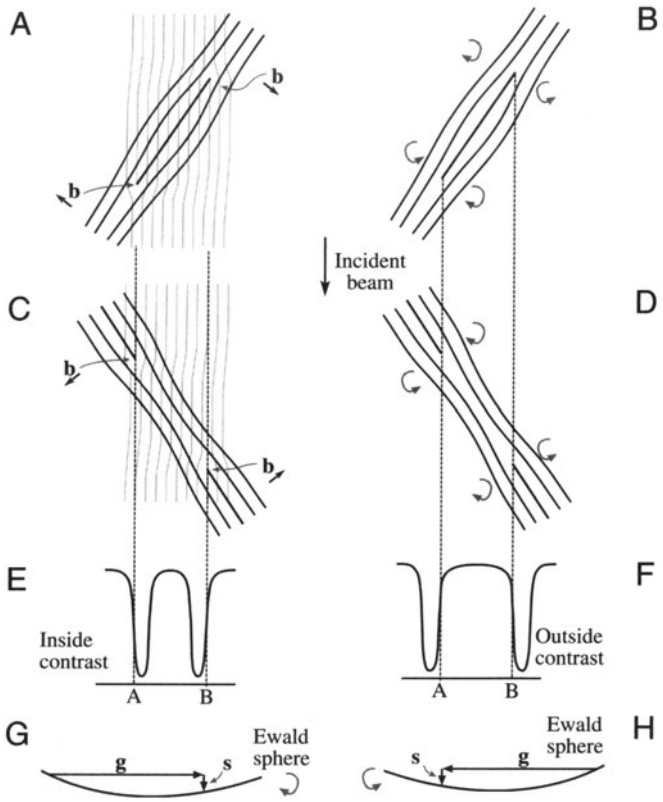

Figure 25.9. (A) Structure of an interstitial loop relative to the diffracting planes (faint lines). (B) Arrows show the rotation of the diffracting planes around the dislocation. (C,D) Vacancy loops. (E,F) Position of the image contrast relative to the projected dislocation position. Inside contrast occurs when clockwise rotation of the diffracting planes brings them into the Bragg condition. Outside contrast occurs for the counterclockwise case. (G,H) The relationship between **g**, **s** and the sense of rotation. Everything is reversed if the loops are tilted in the opposite direction relative to the beam (i.e., reflect this figure in a mirror).

Dislocations in Zn provide a particularly nice illustration of **g**·**b**×**u** contrast. If the specimen surface is parallel to the (0001) basal plane, then dislocation loops can readily form by coalescence of vacancies. In Figure 25.11, **b** is normal to **g** so that **g**·**b** = 0. These loops give a clear illustration of how the appearance of the image depends on the line direction, **u**, of a dislocation. Note that you can see the dislocation, even though **g**·**b** is zero, so this is not an absolute criterion for invisibility.

The above discussion is fine if the loops are large, but a problem arises when they are small. You must then consider the details of the contrast mechanism.

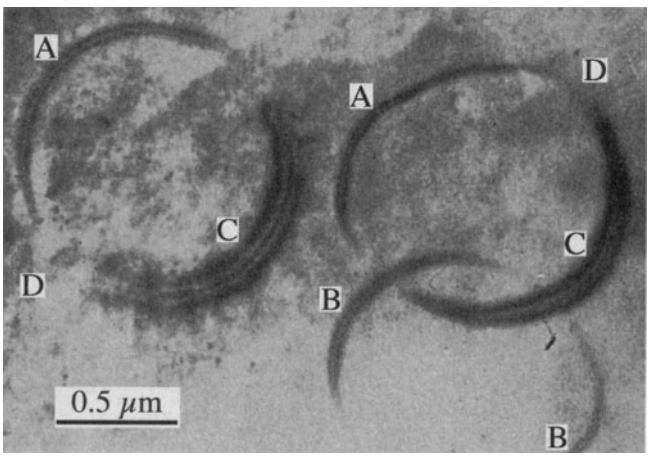

Figure 25.11. Prismatic loops in Zn parallel to the (0001) surface of the specimen with **b** = *c*[0001]. All round the loop, **b** is normal to **g** so that **g**·**b** = 0 and the vector **b**×**u** lies in the plane of the loop. At A, B, and C, **b**×**u** is parallel to **g** so that we see strong contrast. However, at D, **b**×**u** and **g** are mutually perpendicular so that **g**·**b**×**u** = 0 and the loop disappears.

The basic idea is that the appearance of the image is now dependent on the thickness of the specimen.

This was, of course, true for all these images, but now the size of the defect is small compared to the extinction distance. The schematic shown in Figure 25.12 summarizes the contrast which arises from small vacancy loops; if the loops were interstitial in nature, the contrast would be reversed. Not only does the black/white contrast change as the position of the defect changes in the specimen, but its size also appears to change. When the nature of the loops becomes more complex, the appearance of the image may also become more difficult to interpret with "butterflies," "lozenges," and "peanuts" being common terms. Notice that the behavior of the contrast differs in BF and DF images; this effect is similar to that which we discussed in Chapter 24 and is again related to anomalous absorption. A detailed description of this complex contrast behavior is given by Wilkens (1978).

Dislocation dipoles can be present in great numbers in heavily deformed metals, but can also be important in the degradation of some semiconductor devices. Dipoles can be thought of as loops which are so elongated that they look like a pair of single dislocations of opposite Burgers vectors, lying on parallel glide planes. As a result, they are best recognized by their "inside–outside" contrast as illustrated in Figure 25.13. You can appreciate the origin of the term by looking at the projection of the images of the two dislocations when you reverse the sign of **g**: since the two dislocations have opposite Burgers vectors, Figure 25.9 tells you that one image will lie on one side of the core and the other on the opposite side. The order reverses when you reverse **g**.

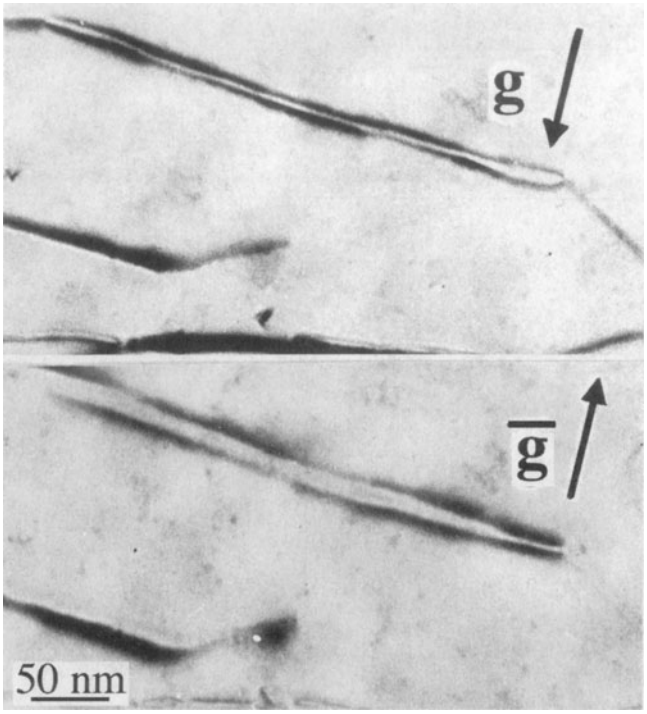

Figure 25.13. Images of dislocation dipoles in Cu showing inside–outside contrast on reversing **g** (±220).

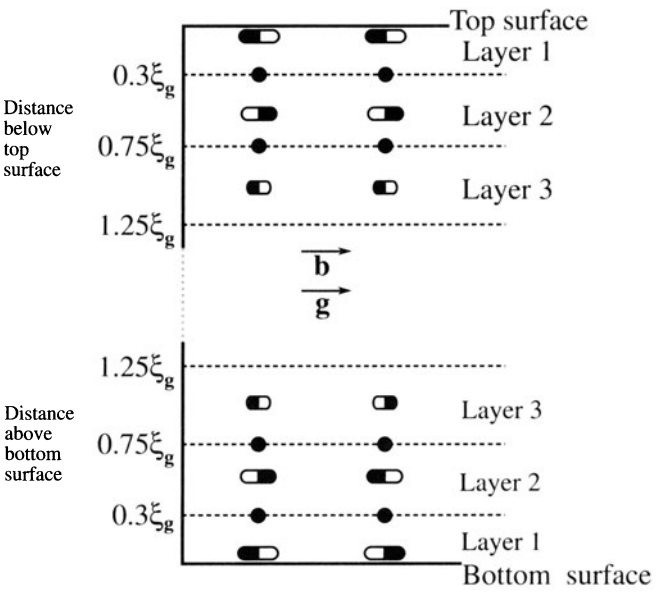

Figure 25.12. Changes in the black–white contrast from small dislocation loops at different layer depths in the specimen. The DF shows the same contrast at the top and bottom while the BF contrast is complementary at the two surfaces.

25.7. DISLOCATION PAIRS, ARRAYS, AND TANGLES

Remember, you are not limited to **g**-vectors which are parallel to the foil surface; hence you can tilt the specimen to see SF contrast. As we saw in Figure 25.8, this is often helpful if you have SFs associated with the dislocations; you can then produce **g**·**R** contrast for the fault. We will discuss dislocation dissociation more in Chapter 26. If you look back at Figure 25.6, you will see the benefit of being able to see the SF. This figure also illustrates the effect of n on the dislocation contrast.

Consider a dislocation in an fcc metal which can dissociate into two Shockley partial dislocations on the (111) plane. We can write down the dislocation reaction as

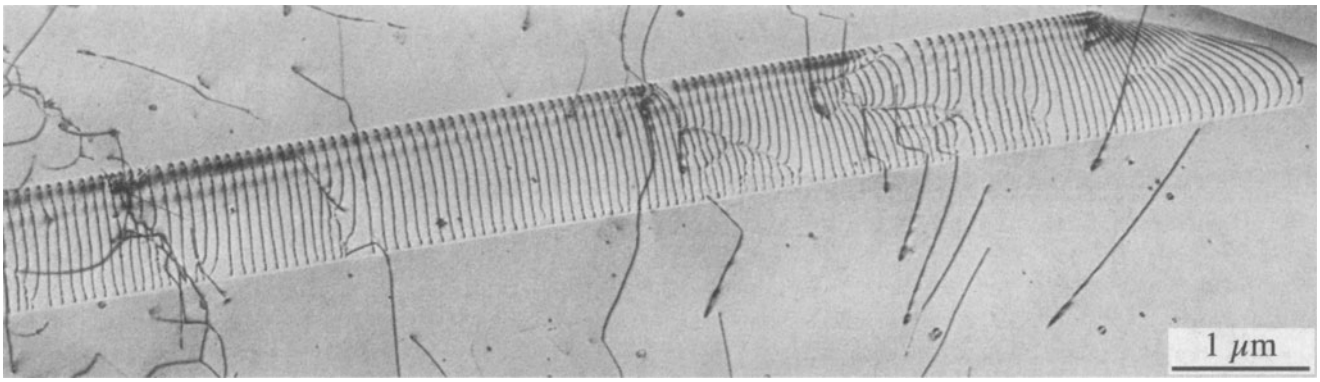

Figure 25.14. Dislocations threading through a very thick specimen in an image recorded using a high-voltage TEM.

$$\frac{1}{2}\left[1\bar{1}0\right] = \frac{1}{6}\left[1\bar{2}1\right] + \frac{1}{6}\left[2\bar{1}\bar{1}\right] \quad \text{on} \left(111\right) \qquad [25.13]$$

If we image this dislocation using the $(2\bar{2}0$ reflection, then $\mathbf{g}\cdot\mathbf{b} = 2$. If, instead, we use the $(20\bar{2})$ reflection, then $\mathbf{g}\cdot\mathbf{b} = 1$. The appearance of the image is very different even if we cannot see the individual partial dislocations.

The advantage of using high voltages to study arrays of dislocations is illustrated in Figure 25.14; everything we said in Chapter 11 applies when we study dislocations. We see thickness fringes at the surface, but these disappear in the central region of the foil. When the foils are this thick, you may find stereomicroscopy helpful in giving a 3D view of the defect arrangement; you can imagine its value in interpreting an image such as that shown in Figure 25.15A. The defects may be very close together in heavily deformed materials, as shown in Figure 25.15B; you then need to make the specimen thin over very large areas to minimize image overlap (e.g., Hughes and Hansen 1995). If the density of defects is too large, the weak-beam technique may be the only way to "look into" the walls (Chapter 26).

25.8. SURFACE EFFECTS

In TEM, we always have thin foils. Dislocation strain fields are long range, but we often assign them a cut-off radius of ~50 nm. However, the thickness of the specimen might only be 50 nm or less, so we can expect the surface to affect the strain field of the dislocation, and vice versa.

When an edge dislocation lies parallel to the surface of a very thin specimen, it causes the specimen to bend. The effect is not large, but large enough compared to the Bragg angle, as illustrated schematically and with an example in Figure 25.16 (Amelinckx 1964).

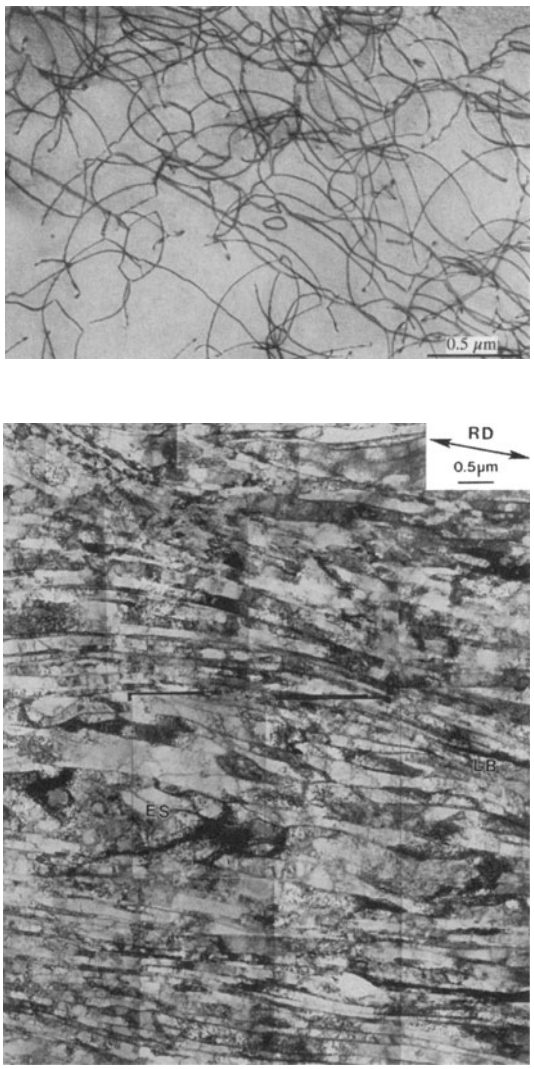

Figure 25.15. (A) Dislocation tangles in an Fe-35% Ni-20% Cr alloy, creep tested at 700°C; the dislocations have moved by glide and climb and do not lie on well-defined planes. (B) Dislocation walls in Al which has been heavily deformed by directional rolling.

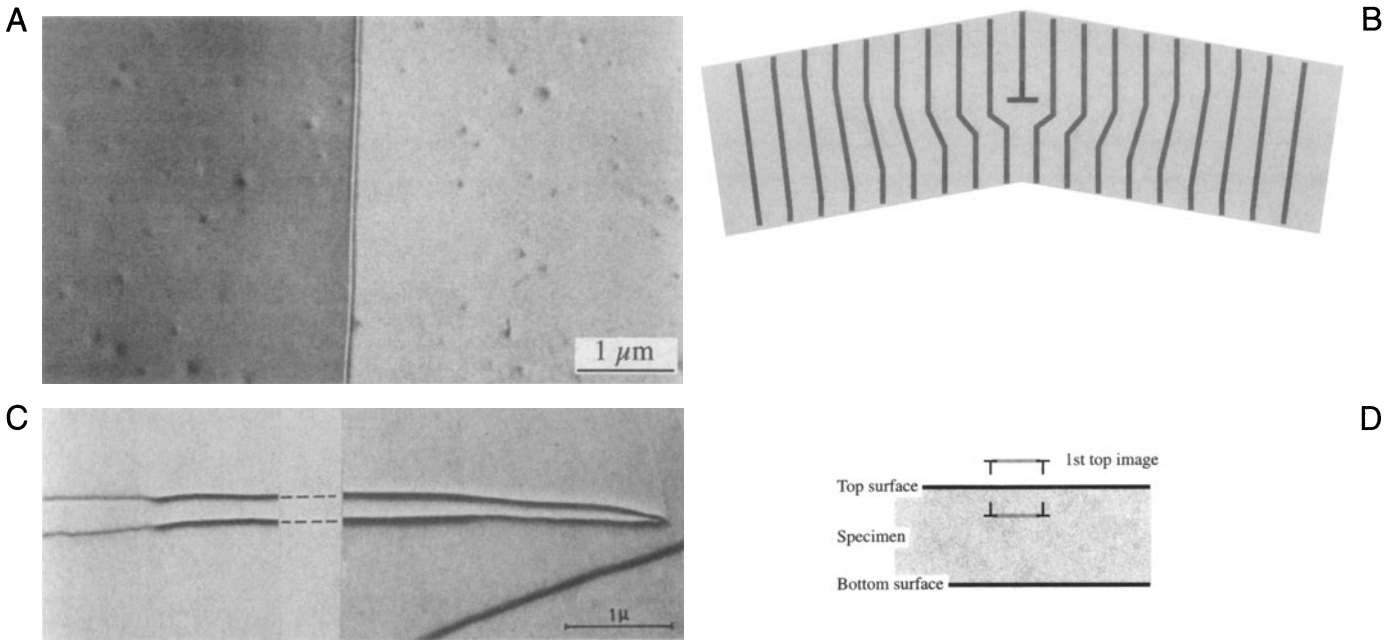

Figure 25.16. (A) A single-edge dislocation lying parallel to the surface of a very thin foil of $SnSe_2$ causes the diffracting planes to bend (B) so we see different intensity in the matrix on either side of the defect. (C,D) If the dislocation is dissociated, the image forces due to the surface cause its width to decrease. The schematic in (D) shows the image dislocations included to represent the effect of the surface.

A calculation: *Sin $\theta_D/2 = \mathbf{b}/2t$. If $\mathbf{b}$ ~ 0.25 nm and t = 50 nm, sin $\theta_D/2 = 0.0025$ and $\theta_D = 0.29^\circ$, which you can compare to a Bragg angle from sin $\theta_B = (n\lambda/2d)$ (0.0037 nm/0.05 nm = 0.0074). $\theta_B = 0.42^\circ$. Notice how θ_D increases for thinner foils and θ_B decreases for increasing voltage (decreasing λ).*

Similarly, if the dislocation is dissociated, the proximity of the surface causes its width to decrease. We can model this situation using "image dislocations" as shown in Figures 25.16C and D. The main point is that we can think of these image dislocations as forcing the partial dislocations closer together; the proximity of the surface can really change the structure of the defect, not just its contrast. A similar effect can occur when the dislocation is inclined to the surface and can result in a V-shaped geometry, as we'll show in Section 26.8.

A special interaction between dislocations and surfaces occurs when a dislocation tries to glide out of the material but can't penetrate a surface layer (which might even be amorphous as in the case of oxide films on metals), as shown in Figure 25.17.

Takayanagi (1988) has shown that we can have dislocations at the surface just because the structure of the surface layer is different from that of the bulk material. The surface of materials can actually reconstruct. The surface of a (111) Au film is more dense than the rest of the film and this misfit is accommodated by surface dislocations, as shown in Figure 25.18. We see the contrast because the strain field extends into the bulk layer. The identification of these dislocations has been confirmed using STM, which also gives more information on the detailed surface structure. However, they were observed first by TEM. The difficulty in TEM studies is that the surface contaminates unless you operate under UHV conditions.

Dislocation can be viewed nearly parallel to their line directions, when we still see contrast even for screw dislocations, as you can see in Figure 25.19A (Tunstall *et al.* 1964). Initially, this contrast is surprising since $\mathbf{g}\cdot\mathbf{b}$ and $\mathbf{g}\cdot\mathbf{b}\times\mathbf{u}$ must be zero for any screw dislocation. However, the screw dislocation can relax at the surface, as shown in Figure 25.19B (Amelinckx 1992).

25.9. DISLOCATIONS AND INTERFACES

Interfaces are, of course, important in all polycrystalline materials. In metals, semiconductors, and thin films on substrates the interaction between dislocations and interfaces is critical. So now we'll briefly examine the special features we see when combining line and planar defects as illustrated in Figure 25.20. This is one topic where image simulation, which we'll discuss in Section 29.12, is invaluable.

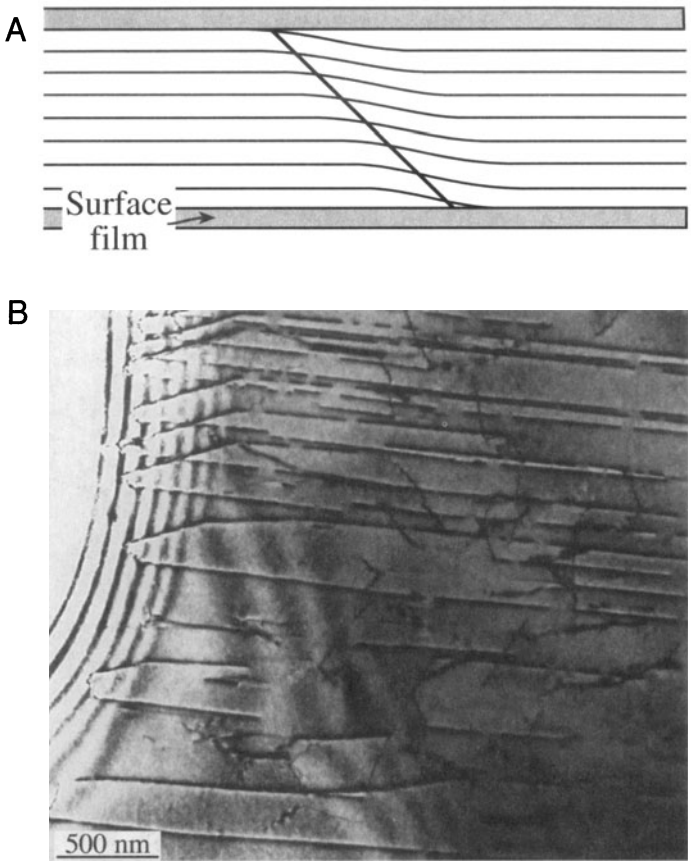

Figure 25.17. (A) Schematic diagram of dislocations pinned at the surface of the specimen by surface films such as oxides. (B) A reduced (i.e., metal) film on NiO pins dislocations. Such films may be introduced during or after thinning to electron transparency.

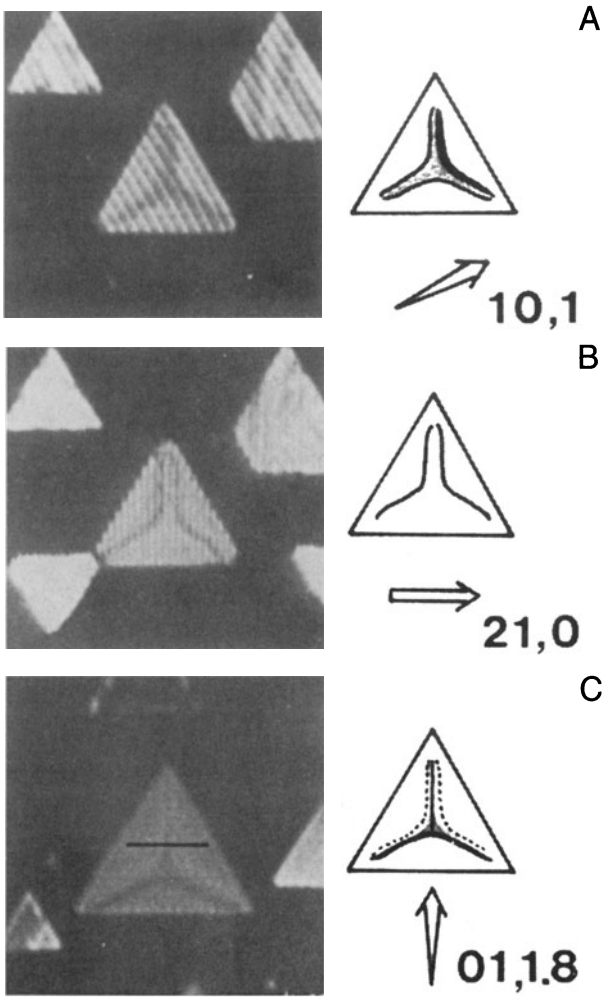

Figure 25.18. Dislocations networks can form at the surface of (111) Au islands because the surface layer relaxes to a "lattice" parameter which is different from that of the bulk material. Different dislocations are visible under different diffracting conditions (A–C).

When we have an array of dislocations, the strain fields overlap so that the value of $\mathbf{R}(\mathbf{r})$ for each dislocation tends to be reduced. This is the grain boundary model of an interface.

Dislocations can be present at interfaces where the composition, or structure, or both change.

- Misfit dislocations accommodate the difference in lattice parameter between two well-aligned crystalline grains. Surface dislocations (as we saw in Section 25.8) are a special subgroup of misfit dislocations.
- Transformation dislocations are the dislocations which move to create a change in orientation or phase. The $\frac{1}{6}$<112> dislocations in twin boundaries in fcc materials are an example of transformation dislocations (twinning dislocations).

A complication in the analysis of images of interfacial dislocations is that they are often associated with steps in the interface. An example of such steps is shown in Figure 25.21. Sometimes, as is the case for the $\frac{1}{6}$<112> twinning dislocations, the dislocations must introduce a step. In other situations, steps are present but there is no dislocation. The difficulty is that we often encounter all three of these situations at the same time. We will also examine these defects, using weak-beam conditions in Chapter 26 and using HRTEM in Chapter 28.

We will discuss the images first and then, remembering that information must also be present in the DP, we will relate the two.

In many cases that interest us, grain boundaries appear as arrays of dislocations. In general, the grains are misoriented. There are some special cases, as we saw in Chapter 24.

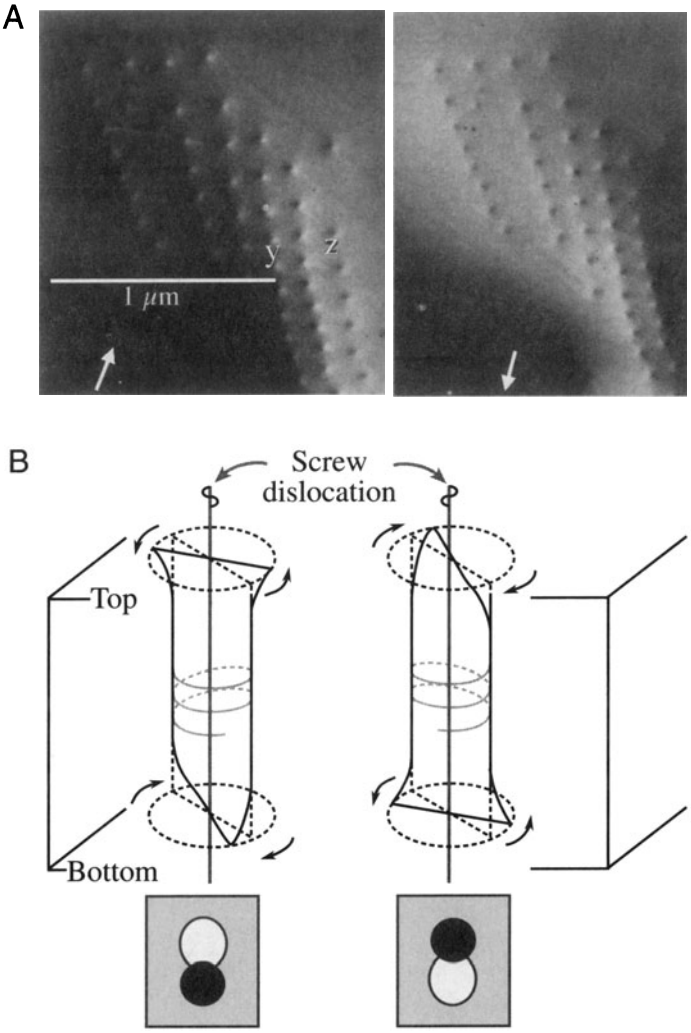

Figure 25.19. (A) Screw dislocations viewed end on (±**g**). The schematics (B) show the diffracting planes rotating in the same direction away from the edge-on orientation at both surfaces.

- Two grains may have a near-common plane and therefore a nearly common, but different, **g**-vector.
- In small-angle grain boundaries, θ is small, so the separation of the dislocations is large ($\sin \theta/2 \cong b/2d$).

The $\Sigma = 3$ twin boundary in fcc materials is an example of an interface where you can use common, but different, **g**-vectors. Here, the $(3\bar{3}\bar{3})$ plane is parallel to the $(\bar{5}11)$ plane, so these two **g**-vectors are identical, as you can see in Figure 25.22. However, this common reflection would not normally be used because **g** is rather large. This coincidence can also occur for other grain boundaries.

In the case of small-angle boundaries, we can pretend that the reflection is common to both grains, as illustrated in Figure 25.23. What we are really doing is treating

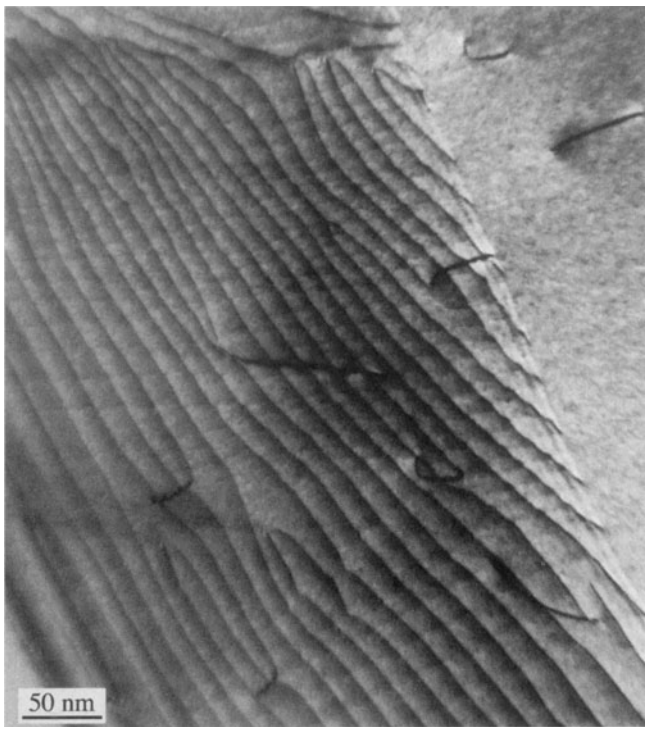

Figure 25.20. Dislocations interacting with a grain boundary; the dislocation contrast changes because its strain field changes when it enters the boundary and becomes part of the dislocation structure.

the dislocations as if they were isolated lattice defects; actually, the **g**-vectors for the two grains will be rotated relative to one another.

Lattice misfit is very important whenever we are studying thin films; dislocations are often present to accommodate the misfit. An example is shown in Figure 25.24, where dislocations are present between spinel and

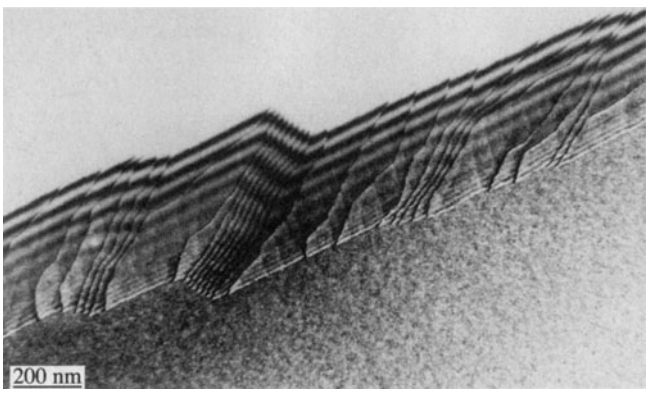

Figure 25.21. Steps at interfaces may also cause diffraction contrast. In this Ge specimen, the steps displace the thickness fringes in the GB. The fringe spacing is different at the top and bottom of the boundary because the diffraction conditions are different in each grain.

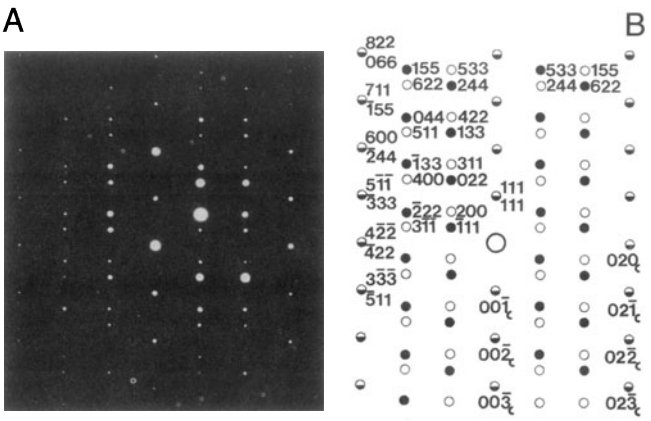

Figure 25.22. (A) DP and (B) its indexed schematic for a $\Sigma = 3$ twin boundary in an fcc material. Notice that many pairs of **g**-vectors exactly overlap but have very different indices.

NiO; these two materials both have the same fcc crystal structure. Although you can easily appreciate the change in lattice parameter, you must remember that there is also a less obvious change in the elastic constants.

> This means that the strain field at phase boundaries is *not* the same as at a grain boundary.

The TEM beam "sees" yet another change: the extinction distance is different. The result is that, if the crystal is inclined to the electron beam, you will see thickness fringes associated with the interface. Not much work has been done on this, but you may find that it is more difficult to use the **g**·**b** criterion for determining Burgers vectors, especially when the misfit is large.

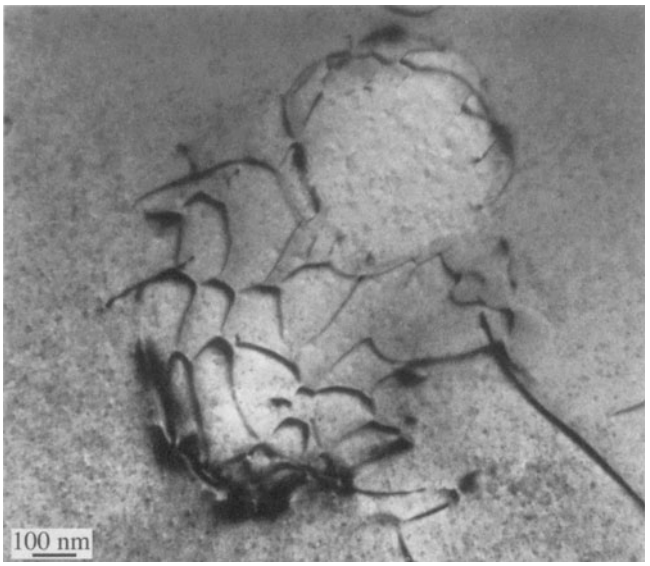

Figure 25.24. An irregular array of misfit dislocations at the interface between a spinel particle and an NiO matrix. The lattice mismatch is very small as you can appreciate from the scale. Although you can "see" a distorted hexagonal array of dislocations, you have to remember that this interface is actually curving within the specimen so that we are only seeing a projection of the structure.

Phase transformations often involve the movement of dislocations generally at semicoherent interfaces. All the conditions discussed above may hold; however, now the dislocations will certainly be associated with a step on the interface, so as to physically translate the interface as the transformation proceeds. However, you will find it dif-

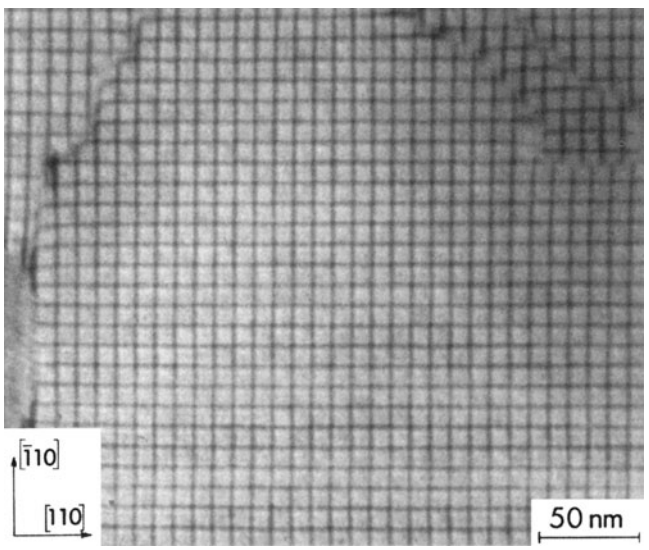

Figure 25.23. A low-angle (001) twist boundary in Si oriented almost exactly parallel to the specimen surface. Two (040) reflections were excited to form this BF image, but for small misorientations these are so close that we treat them as one reflection.

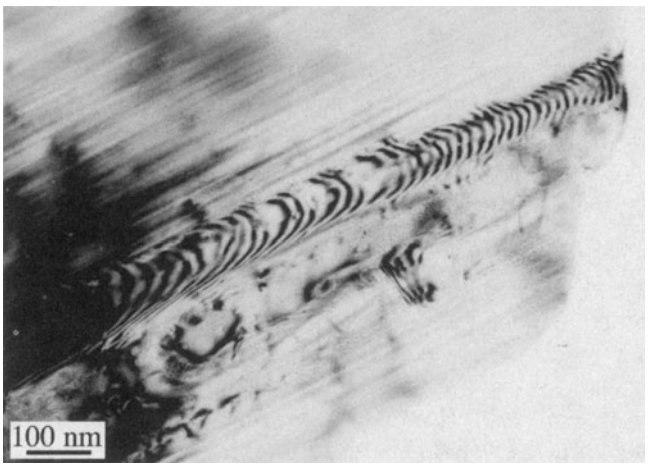

Figure 25.25. Transformation dislocations in the interface between a growing lath of hematite (pseudo-hexagonal alumina structure) in a ferrite (cubic spinel structure) matrix. The dislocations are curved because they were moving while heating the thinned specimen, which is why we know they are transformation dislocations, not simply misfit dislocations.

ficult to model the contrast from such dislocations, especially when you have a thin layer of the new phase enclosed by the matrix, as in the case when a precipitate grows, as illustrated in Figure 25.25.

The main effect of steps on such interfaces is that they cause a shift in the thickness fringes. It is often difficult to tell if there is also a dislocation present.

We'll summarize some features you should remember when studying dislocations in interfaces:

- If the orientation of the grains is different, the distribution of strain from the dislocation may be different in the two grains; the diffraction contrast is determined by this strain field.
- If the chemistry of the two grains is different or if you use different but equal **g**-vectors, the extinction distances will be different and the image of the dislocations must therefore be affected.
- Be careful not to confuse moiré fringes with dislocations (we'll discuss moiré fringes in Chapter 27). The guide is that the dark and light moiré fringes have approximately equal widths; if there is any ambiguity, you should use weak-beam imaging (Chapter 26) and carefully examine the DP.

Humble and Forwood (1975) have shown, using computer simulation of dislocations in interfaces, that it is best to use diffraction conditions where a reflection is satisfied in both grains, otherwise the dislocation images tend to be rather featureless relative to the interface thickness fringes.

25.10. VOLUME DEFECTS AND PARTICLES

When the defects are small, the image may be dominated by the strain-field contrast, and that is the aspect we are considering here. You have to remember, though, that the defects may have a different structure, lattice parameter, and composition. The theory for a spherical particle in a matrix was given over 30 years ago by Ashby and Brown (1963).

> The theory works well for coherent particles but as soon as the first interface dislocation appears, analysis becomes much more difficult.

Lattice-strain effects around spherical precipitates appear as lobes of low intensity with a line of no contrast perpendicular to **g**, as shown in Figure 25.26. If you measure the size of the precipitates from a DF image and the size of the strain-contrast lobes in BF, you can get a direct measure of

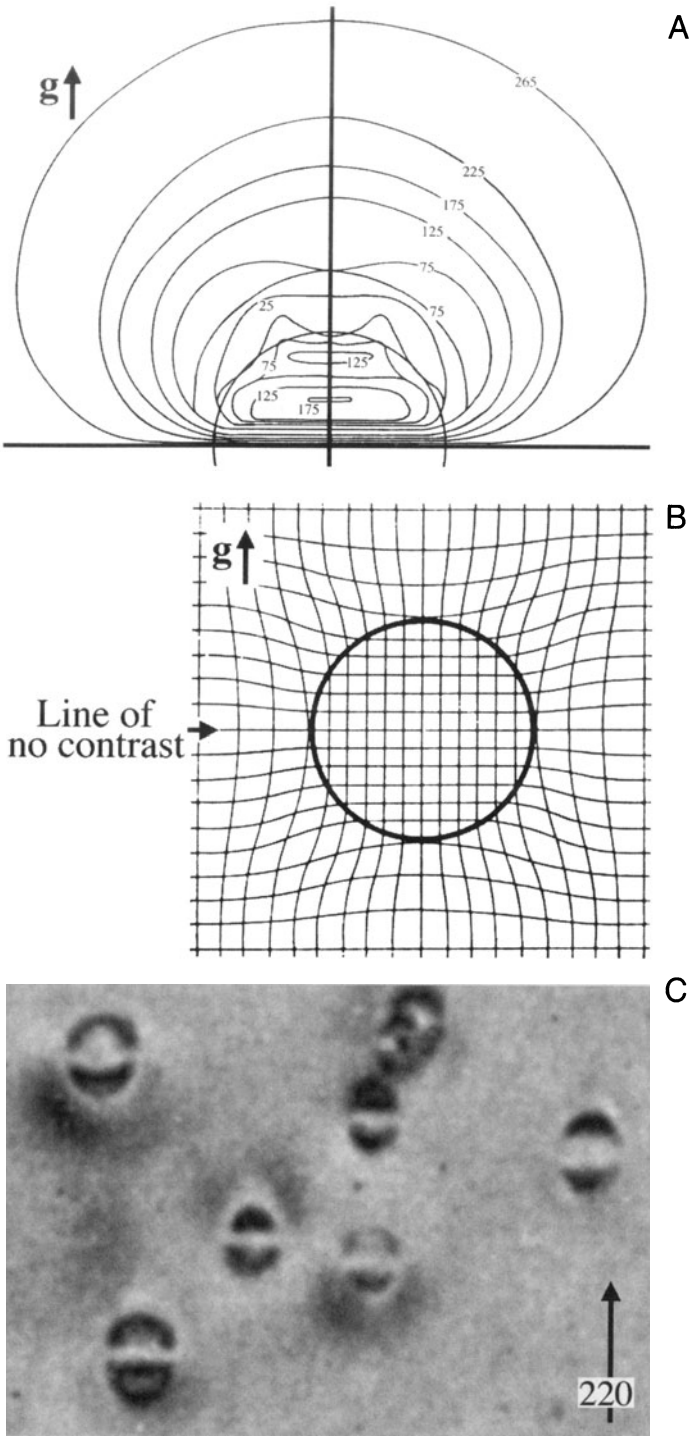

Figure 25.26. (A) Intensity contours from a simulated image of a particle like that shown schematically in (B). Notice the line of no contrast which corresponds to the plane that is not distorted by the strain field of the particle. (C) Experimental image of coherent particles in Cu-Co showing strain contrast.

the lattice strain surrounding a single precipitate, which is really quite remarkable. The process requires some specific experimental conditions and careful calibration of the photographic recording procedure, which there isn't space to describe, so you should read the original references for details. If your precipitates aren't spherical, intuitive interpretation of the images is unreliable and you have to resort to computer simulation.

Figure 25.26B shows how a spherical particle might strain the lattice. Notice that in this case, all the planes continue across the particle so it is coherent and there are no misfit dislocations. The figure here assumes that all the strain occurs in the matrix, which is only true for a hard particle in a soft matrix. The displacement field used to model this situation is

$$\mathbf{R} = C_\varepsilon \mathbf{r} \qquad [25.14]$$

when $\mathbf{r} \leq \mathbf{r}_0$, and

$$\mathbf{R} = C_\varepsilon \frac{r_0^3}{r^3} \mathbf{r} \qquad [25.15]$$

when $\mathbf{r} \geq \mathbf{r}_0$, where C_ε is an expression for the elastic constants, given by

$$C_\varepsilon = \frac{3K\delta}{3K + 2E(1+\nu)} \qquad [25.16]$$

and K is the bulk modulus of the precipitate; E and ν are Young's modulus and Poisson's ratio, respectively, for the matrix. The important feature is that $\mathbf{R}$ always shows radial symmetry. Thus, when we consider the Howie–Whelan equations, we realize that when $\mathbf{g}\cdot\mathbf{R} = 0$ we will see no contrast. So, there will be a "line of no contrast" normal to $\mathbf{g}$.

The strain can be plotted using the equations given by Ashby and Brown and the image simulated (see below) as shown in Figure 25.26A. In the image from a specimen of a Cu-Co alloy containing small Co precipitates shown in Figure 25.26C, we can see that the images of the particles resemble butterflies or coffee beans. With the improvement in computers, the image contrast expected from much more complex particle geometries can now be calculated and can even consider statistical structural fluctuations (e.g., Karth *et al.* 1995).

25.11. SIMULATING IMAGES

It is important that you understand the origins of diffraction contrast from strain fields before you try to simulate this contrast using a computer. Having said that, few students would want to calculate image intensities by hand. The Howie–Whelan equations can be used to simulate images of dislocations, which is especially important when the dislocations are close together. The principal approaches used to simulate diffraction-contrast images were discussed in Sections 24.11 to 24.13.

If you want to make quantitative comparisons with real images recorded on film, you must correct for the nonlinearity of the film (see Chapter 30).

Although the algorithm employed by the Head *et al.* (1973) programs allow very fast computation of the image, it does so by restricting the geometry of the defects. To cope with more general geometries, e.g., the strain field from end-on screw dislocations or nonparallel dislocations, Thölén (1970a) introduced a matrix algorithm. As we saw in Chapter 24, Howie and Basinski (1968) extended the two-beam calculations to include several beams on the systematic row and presented a method for circumventing the column approximation.

25.11.A. The Defect Geometry

When choosing the optimal simulation method, depending on the defect geometry, the problem of calculating the image belongs to one of three categories:

- *Two-dimensional problem:* including the most general geometries where integration of the full two-dimensional (x,y) grid is necessary.
- *One-dimensional problem:* geometries where the image depends only on either x or y and can be represented by a profile, e.g., problems involving a dislocation parallel to the foil surfaces.
- *GCS problem:* geometries where the method of generalized cross sections (GCS), developed by Head *et al.* (1973), can be applied. Situations where the dislocations and fault planes are parallel to each other, but inclined to the foil surface, are included in this group.

Choosing the best method can speed up the simulations considerably, as we'll show later. The Head *et al.* program automatically determines the category and selects the appropriate calculation method.

25.11.B. Crystal Defects and Calculating the Displacement Field

The program Comis can simulate amplitude contrast from any number of defects consisting of fault planes and straight, infinite dislocations (Rasmussen and Carter 1991). You just need to define the Burgers vector, line di-

rection, and relative position; planar faults are defined by the plane normal, the displacement vector, and the relative position. You can predefine certain standard geometries to ease the process of defining the defect system.

Once you've defined the defect geometry, consider the region of the crystal you want to simulate. In situations where the "interesting" region is well defined (as in the case of inclined dislocations or intersecting dislocations), the program will determine this region and provide it as the default. However, you can always set the image region manually in Ångström units, to obtain a desired magnification.

The displacement field for the dislocations is calculated using linear, anisotropic elasticity theory (Eshelby *et al.* 1953) and is based on the algorithms given by Head *et al.* (1973), so you must specify the elastic constants of your crystal. The displacement field then corresponds to straight, infinite dislocations in an infinite medium with no account taken of surface relaxations. You can introduce image dislocations outside the crystal in order to include surface effects.

25.11.C. The Parameters

An example which shows simulated images of an orthogonal network of screw dislocations is given in Figure 25.27. Thölén (1970b) has analyzed this situation in detail. Comis can calculate the equilibrium configuration of certain types of interacting dislocations (Morton and Forwood 1973) using anisotropic elasticity theory, and then directly incorporate the resulting geometry in subsequent image simulations. As you can appreciate from equation 25.5, in such simulation studies, you will need *all* the parameters for the defects, the specimen, and the diffraction conditions:

- The foil thickness.
- The stacking-fault energy.
- The absorption parameters, usually using $|U_g'|/|U_g| = 0.1$.
- The number of beams included in the calculation.

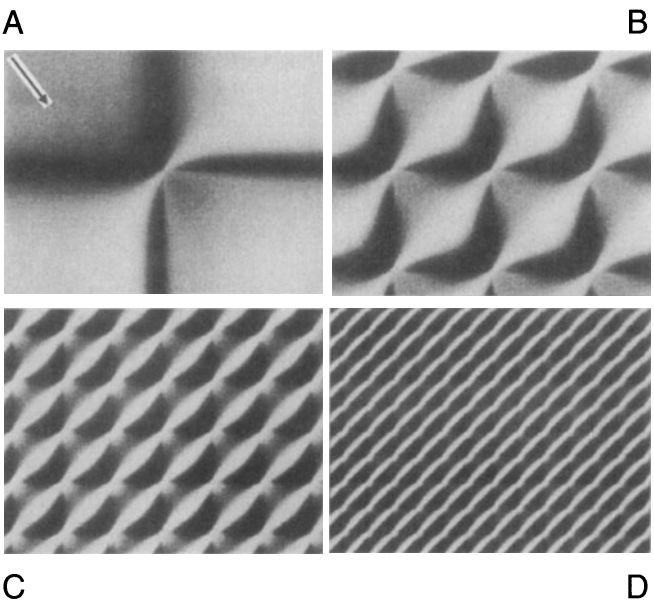

Figure 25.27. Simulated two-beam BF images of networks of screw dislocations, located in the middle of a foil with thickness equal to 4 times the extinction distance, ξ_g; $\mathbf{g}\cdot\mathbf{b} = 1$ for both dislocation types. The separation between the dislocations is: (A) ∞, (B) $1\xi_g$, (C) $0.5\xi_g$, (D) $0.25\xi_g$.

- The zone axis and the diffracting vectors.
- Also required are the electron energy, the elastic constants, the normal to the foil surface, the Burgers vectors, and the line direction of the dislocations.

The exact beam direction is then specified by defining the "center" of the Laue zone, giving the coordinates in terms of the **g** vector and $\mathbf{g}_z$. Here $\mathbf{g}_z$ is a specially defined vector in reciprocal space, which is automatically set to lie in the ZOLZ and to be perpendicular to **g**. Thus, if you place the center of the ZOLZ at (0, 0), the specimen is oriented on the zone axis; if you place the center of the ZOLZ at (0.5, 0), it corresponds to being at **g**/2, i.e., at the Bragg position with the **0** and **g** beams excited. If you change the second coordinate to give, say, (0.5, 0.5), you need to include beams from off the systematic row.

CHAPTER SUMMARY

The central idea of this chapter is that the strain field moves atoms off their perfect-crystal positions. We've concentrated on dislocations because the edge dislocation gives the clearest illustration of how the deformation produces the contrast and its structure can be understood with a two-dimensional projection. We can summarize the topics of the chapter as follows:

- There is a new feature to the column approximation. The displacement moves atoms out of the column and brings others into the column.

- The basis of the **g·b** analysis of dislocations is simply that the contrast is determined by **g·R(r)** and that **R(r)** is linearly related to **b**. For the screw dislocation, **R(r)** is directly proportional to **b**. For the edge dislocation, the image can also be affected by a **g·b×u** component which is caused by the buckling of the dislocation glide plane.
- Dislocation images are usually asymmetric. The contrast depends on the sign of $(\mathbf{g}\cdot\mathbf{b})s$.
- As a practical rule, we usually set **s** to be >0. Then the distortion due to the defect will bend the near-diffracting planes back into the Bragg-diffracting condition to give strong contrast. When $\mathbf{s} > 0$, detail in the image is more localized relative to the defect than if we use the $\mathbf{s} = 0$ condition.

There are many other situations which are closely related to the topics we've discussed in this chapter. For example, we have not discussed strain contrast associated with crack tips (de Graf and Clarke 1993) or the analysis of buckling of thin specimens (Thölén and Taftø 1993). Although these are rather specialized situations, they do illustrate the growing applications of diffraction contrast in the TEM.

REFERENCES

General References

Amelinckx, S. (1964) *The Direct Observation of Dislocations,* Academic Press, New York. A fascinating summary of the early studies by TEM.

Amelinckx, S. (1979) in *Dislocations in Solids,* 2 (Ed. F.R.N. Nabarro), North-Holland, New York. If you're interested in dislocations there are many other volumes in this set.

Amelinckx, S. and Van Dyck, D. (1992) in *Electron Diffraction Techniques,* **2** (Ed. J.M. Cowley), p. 1, Oxford University Press, New York.

Edington, J.W. (1976) *Practical Electron Microscopy in Materials Science,* Van Nostrand Reinhold, New York.

Head, A.K., Humble, P., Clarebrough, L.M., Morton, A.J., and Forwood, C.T. (1976) *Computed Electron Micrographs and Defect Identification,* North-Holland, New York.

Hirsch, P.B., Howie, A., Nicholson, R.B., Pashley, D.W., and Whelan, M.J. (1977) *Electron Microscopy of Thin Crystals,* 2nd edition, Krieger, Huntington, New York.

Hirth, J.P. and Lothe, J. (1982) *Theory of Dislocations,* 2nd edition, John Wiley & Sons, New York. The definitive textbook, but not for the beginner.

Hull, D. and Bacon, D.J. (1984) *Introduction to Dislocations,* 3rd edition, Pergamon Press, New York. A great introductory text.

Matthews, J.W., Ed. (1975) *Epitaxial Growth,* Parts A and B, Academic Press, New York.

Nabarro, F.R.N. (1987) *Theory of Dislocations,* Dover Publications, New York.

Porter, D.A. and Easterling, K.E. (1992) *Phase Transformations in Metals and Alloys,* 2nd edition, Chapman and Hall, New York.

Smallman, R.E. (1985) *Modern Physical Metallurgy,* 4th edition, Butterworth-Heinemann, Boston.

Sutton, A.P. and Balluffi, R.W. (1995) *Interfaces in Crystalline Materials,* Oxford University Press, New York.

Wolf, D. and Yip, S., Eds. (1992) *Materials Interfaces: Atomic-Level Structure and Properties,* Chapman and Hall, New York. A collection of review articles.

The original series of papers by P.B. Hirsch, A. Howie, M.J. Whelan, and H. Hashimoto in *Proc. Roy. Soc. London* **A252**, 499 (1960), **263**, 217 (1960), **267**, 206 (1962), and **268**, 80 (1962) are strongly recommended.

Specific References

Amelinckx, S. (1992) in *Electron Microscopy in Materials Science* (Eds. P.G. Merli and M.V. Antisari), World Scientific, River Edge, New Jersey.

Ashby, M.F. and Brown, L.M. (1963) *Phil. Mag.* **8**, 1083 and 1649.

de Graf, M. and Clarke, D.R. (1993) *Ultramicroscopy* **49**, 354.

Eshelby, J.D., Read, W.T., and Shockley, W. (1953) *Acta Metall.* **1**, 251.

Goringe, M.J. (1975) in *Electron Microscopy in Materials Science* (Eds. U. Valdrè and E. Ruedl), p. 555, Commission of the European Communities, Luxembourg.

Hirsch, P.B., Howie, A., and Whelan, M.J. (1960) *Phil. Trans. Roy. Soc.* **A252**, 499.

Howie, A. and Basinski, Z.S. (1968) *Phil. Mag.* **17**, 1039.

Howie, A. and Sworn, H. (1970) *Phil. Mag.* **31**, 861.

Hughes, D.A. and Hansen, N. (1995) *Scripta Met. Mater.* **33**, 315.

Humble, P. and Forwood, C.T. (1975) *Phil. Mag.* **31**, 1011 and 1025.

Karth, S., Krumhansl, J.A., Sethna, J.P., and Wickham, L.K. (1995) *Phys. Rev. B* **52**, 803.

Morton, A.J. and Forwood, C.T. (1973) *Cryst. Lattice Defects* **4**, 165.

Rasmussen, D.R. and Carter, C.B. (1991) *J. Electron Microsc. Technique* **18**, 429.

Steeds, J.W. (1973) *Anisotropic Elastic Theory of Dislocations,* Clarendon Press, Oxford, United Kingdom.

Takayanagi, K. (1988) *Surf. Sci.* **205**, 637.

Thölén, A.R. (1970a) *Phil. Mag.* **22**, 175–182.

Thölén, A.R. (1970b) *Phys. Stat. Sol. (a)* **2**, 537.

Thölén, A.R. and Taftø, J. (1993) *Ultramicroscopy* **48**, 27

Tunstall, W.J., Hirsch, P.B., and Steeds, J.W. (1964) *Phil. Mag.* **9**, 99.

Wilkens, M. (1978) in *Diffraction and Imaging Techniques in Material Science,* 2nd edition (Eds. S. Amelinckx, R. Gevers, and J. Van Landuyt), p. 185, North-Holland, New York.